≪연구논문≫ Journal of the Korean Magnetics Society, Volume 22, Number 3, June 2012 http://dx.doi.org/10.4283/JKMS.2012.22.3.085

$Nd_2Fe_{14}B$ 화합물 결정의 산화 및 보자력에 관한 연구

권해웅*
부경대학교, 부산시 남구 용당동 산100번지, 608-739

유지훈
한국재료연구소, 경남 창원시 성산구 창원대로 797, 641-831

(2012년 6월 11일 받음, 2012년 6월 19일 수정본 받음, 2012년 6월 19일 게재확정)

$Nd_2Fe_{14}B$ 화합물 결정의 산화 및 미세 $Nd_2Fe_{14}B$ 결정입자의 보자력에 미치는 산화의 영향을 조사하였다. $Nd_2Fe_{14}B$ 화합물 결정의 산화속도는 $Nd_{15}Fe_{77}B_8$ 합금 잉곳 중의 과잉 성장시킨 $Nd_2Fe_{14}B$ 결정립을 이용하여 조사하였다. $Nd_2Fe_{14}B$ 화합물 결정의 산화는 이 결정상의 α-Fe, Fe_3B, 및 Nd 산화물 복합상으로의 분해에 의해 일어 났다. $Nd_2Fe_{14}B$ 화합물 결정의 산화속도는 결정 방위와는 무관하였다. 산화반응 속도 식은 단순한 직선관계로 나타났다. $Nd_2Fe_{14}B$ 화합물 결정의 산화에 대한 활성화에너지는 약 26.8 kJ/mol로 계산되었다. HDDR 처리한 $Nd_{15}Fe_{77}B_8$ 합금을 볼밀링하여 임계단자구 크기에 유사한 미세한 $Nd_2Fe_{14}B$ 결정입자를 제조하고, 이 입자들을 이용하여 보자력에 미치는 산화의 영향을 조사하였다. 임계단자구 크기에 유사한 미세한 $Nd_2Fe_{14}B$ 결정입자(≒0.3 μm)는 9 kOe 이상의 높은 보자력을 가졌다. 그러나, 이 보자력은 공기 중에서 온도 상승에 따라 급격하게 저하하였다(200 ºC에서 2 kOe 이하). 이러한 급격한 보자력의 감소는 산화에 의해 미세 입자의 표면에 형성된 연자성 α-Fe 및 Fe_3B 상 때문으로 판단되었다.

주제어 : Nd-Fe-B 자석, $Nd_2Fe_{14}B$ 결정, 산화, 보자력

Study on Oxidation and Coercivity of $Nd_2Fe_{14}B$ Compound Crystal

H. W. Kwon*
Pukyong National University, Nam-Gu, Busan 608-739, Korea

J. H. Yu
Korea Institute of Materials Science, Changwon 641-831, Korea

(Received 11 June 2012, Received in final form 19 June 2012, Accepted 19 June 2012)

Oxidation of the $Nd_2Fe_{14}B$ compound crystal and its effect on the coercivity of the fine $Nd_2Fe_{14}B$ crystal particles were investigated. Oxidation kinetics of the $Nd_2Fe_{14}B$ compound crystal was investigated using an excessively grown $Nd_2Fe_{14}B$ grains in the $Nd_{15}Fe_{77}B_8$ alloy ingot. Oxidation of the $Nd_2Fe_{14}B$ compound crystal occurred by dissociation of the phase into multi-phase mixture of α-Fe, Fe_3B, and Nd oxides. Oxidation rate of the $Nd_2Fe_{14}B$ compound crystal showed no dependence on the crystallographic direction. The oxidation reaction was modeled according to simple linear relationship. Activation energy for the oxidation of $Nd_2Fe_{14}B$ compound crystal was calculated to be approximately 26.8 kJ/mol. Fine $Nd_2Fe_{14}B$ crystal particles in near single domain size was prepared by ball milling of the HDDR-treated $Nd_{15}Fe_{77}B_8$ alloy, and these particles were used for investigating the effect of oxidation on the coercvity. The near single domain size $Nd_2Fe_{14}B$ crystal particles (≒0.3 μm) had high coercivity over 9 kOe. However, the coercivity was radically reduced as the temperature increased in air (<2 kOe at 200 ºC). This radical coercivity reduction was attributed to the soft magnetic phases, α-Fe and Fe_3B, which were formed on the surface of the fine particles due to the oxidation.

Keywords : Nd-Fe-B magnet, $Nd_2Fe_{14}B$ crystal, oxidation, coercivity

*Tel: (051) 629-6362, E-mail: hwkwon@pknu.ac.kr

I. Introduction

Nd-Fe-B-type magnet has been most widely used in the high performance permanent magnet applications, and the high performance of Nd-Fe-B-type magnet is due to the superior magnetic properties of the matrix $Nd_2Fe_{14}B$ magnetic crystal in the magnet [1, 2]. Since the $Nd_2Fe_{14}B$ compound contains high content of rare earth Nd, which has great affinity with oxygen, the matrix $Nd_2Fe_{14}B$ magnetic crystal in the Nd-Fe-B-type magnet is prone greatly to an oxidation. The oxidation issue of the Nd-Fe-B material has been increasingly raised due to an increased service temperature of the magnets and to an increased need of fine $Nd_2Fe_{14}B$ magnetic crystal particles for various applications [3-5]. In order to understand fully the oxidation of the Nd-Fe-B-type magnets and fine powder, a knowledge about oxidation of the $Nd_2Fe_{14}B$ compound crystal is essential. In the present study, the oxidation kinetics of $Nd_2Fe_{14}B$ compound crystal was investigated, and the effect of oxidation on the coercicity of the fine $Nd_2Fe_{14}B$ particles was investigated.

II. Experimental Work

Oxidation of the $Nd_2Fe_{14}B$ compound crystal was investigated using an excessively grown $Nd_2Fe_{14}B$ grains in the $Nd_{15}Fe_{77}B_8$ alloy ingot. The $Nd_{15}Fe_{77}B_8$ alloy button was prepared by arc-melting of the constituent elements, and the prepared button was homogenized at 1343 K for prolonged period of 4 days under Ar gas in an attempt to cause a full grain growth of the $Nd_2Fe_{14}B$ grains in the alloy. After the prolonged annealing, some $Nd_2Fe_{14}B$ grains were grown markedly to a size ranging from 50 to 300 μm in diameter. Cubic specimen with dimension of 8 × 8 × 8 mm was cut from the annealed ingot, and the surface of the cube was polished. The polished sample was exposed to air at the temperature ranging from 623 K to 723 K. The oxidation kinetics of the $Nd_2Fe_{14}B$ crystal was examined by measuring the thickness of oxidized layer on the surface of $Nd_2Fe_{14}B$ grain. The oxidized layer was observed by optical microscope (OM) with polarized light and scanning electron microscope (SEM). The thickness of the oxidized layer was obtained by taking an average value from ten different crystals. Dependence of oxidation rate upon the crystallographic direction in the $Nd_2Fe_{14}B$ crystal was examined. Crystallographic orientation of the $Nd_2Fe_{14}B$ grains was determined by observing the magnetic domain image of the polished flat surface of individual grain using Kerr effect. Phase analysis of the oxidized layer was carried out by XRD. Specimen for the XRD phase analysis was prepared by oxidizing the fine particles of the $Nd_{15}Fe_{77}B_8$ alloy. The effect of surface oxidation on the coercivity of the fine $Nd_2Fe_{14}B$ crystal particles was investigated using particles with near single domain size which were prepared by roller ball milling (4 hr) of the HDDR-treated $Nd_{15}Fe_{77}B_8$ alloy. Details of HDDR-treatment and ball milling of this alloy can be found elsewhere [6]. Coercivity of the particles was measured by VSM.

III. Results and Discussion

Fig. 1 shows the oxidized layer formed on the surface of the $Nd_2Fe_{14}B$ crystal grains with different crystallographic orientation in the $Nd_{15}Fe_{77}B_8$ alloy. The magnetic domain image (Kerr image) of individual $Nd_2Fe_{14}B$ crystal grains shown in Fig. 1 can provide a clue for determining the approximate crystallographic orientation of the individual grain. A magnetic crystal with uniaxial magnetocrystalline anisotropy exhibits a unique magnetic domain image depending on the crystallographic orientation. The $Nd_2Fe_{14}B$ compound crystal has tetragonal structure and uniaxial

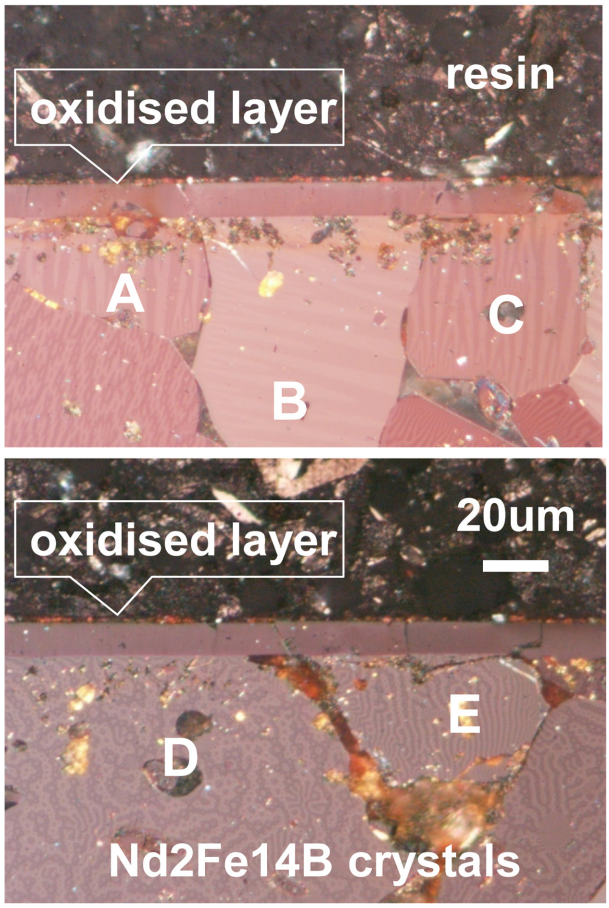

Fig. 1. (Color online) Oxidized layer and magnetic domain image (Kerr image) of the $Nd_2Fe_{14}B$ crystal grains in the $Nd_{15}Fe_{77}B_8$ alloy oxidized at 673 K for 3 hrs.

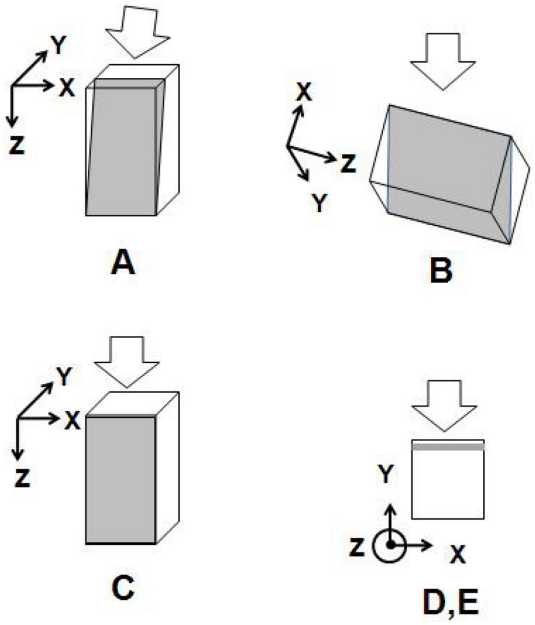

Fig. 2. Schematic showing the oxidation progress directions on various crystallographic planes of the (A) to (E) $Nd_2Fe_{14}B$ crystal grains observed in Fig. (1).

magnetocrystalline anisotropy with its *c*-axis being the easy magnetization axis (EMA). The plane with the 'cogwheel'-type domain image is the basal plane (00l) of the tetragonal crystal which is perpendicular to the EMA (see grain D, E in Fig. 1). Meanwhile, the plane with 'cigar'-type image is the plane parallel to the EMA (*c*-axis) and indexed as (hk0). The longitudinal direction of the cigar-type stripe is the same as the EMA (*c*-axis) (like grain B, C in Fig. 1). The planes with certain angle in between 0^o and 90^o with respect to the major directions of [001] or [u00] or [uv0] may exhibit the magnetic domain image which is slightly elongated and distorted cogwheel- or cigar-type image depending on the angle (like grain A in Fig. 1). Fig. 2 shows schematically the oxidation progress direction (indicated by arrow) on the planes observed in Fig. 1. The highlighted planes are corresponding to one of the probable crystallographic planes determined from the domain image observation in Fig. 1. It can be seen that a continuous oxidized layer has been formed on the surface of each $Nd_2Fe_{14}B$ crystal grain. It appears that the oxidized layer thickness on the various crystal grains is almost identical regardless of the crystallographic orientation. This indicates obviously that the oxidation rate of the $Nd_2Fe_{14}B$ crystal shows no dependence on the crystallographic direction. No dependence of the oxidation on the crystallographic orientation can be explained by a unique oxidation reaction of the $Nd_2Fe_{14}B$ crystal in air. The oxidation of $Nd_2Fe_{14}B$ crystal has been known to takes place by a dissociation of the

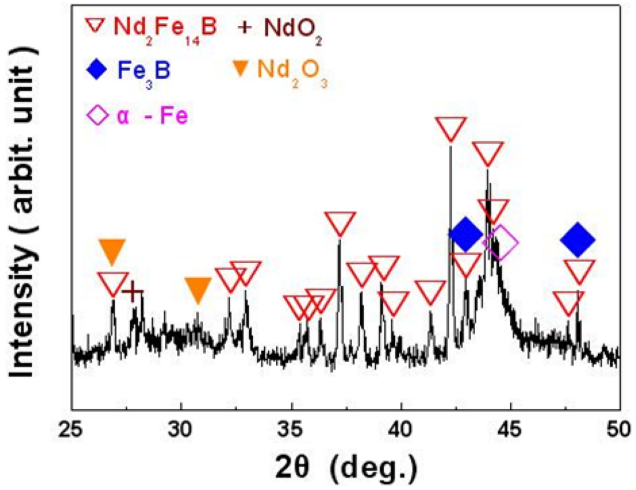

Fig. 3. (Color online) XRD result of the fine $Nd_2Fe_{14}B$ crystals oxidized at 673 K for 3 hrs.

$Nd_2Fe_{14}B$ [3, 4]. Thermodynamic stability of the $Nd_2Fe_{14}B$ phase at an elevated temperature in an oxygen atmosphere (air) is reduced, and the phase is dissociated into a thermodynamically more stable mixture of α-Fe, Fe_3B, and Nd-oxides. Phase constitution in the oxidation product was examined using fine $Nd_2Fe_{14}B$ crystal powder oxidized at 673 K for 3 hrs, and the XRD phase analysis result was shown in Fig. 3. It appears that the oxidized powder consists of multi-phase mixture of $Nd_2Fe_{14}B$, α-Fe, Fe_3B, and Nd oxides. This indicated that at the surface outer shell of the fine $Nd_2Fe_{14}B$ crystal oxygen induced a dissociation of the $Nd_2Fe_{14}B$ phase into the mixture of α-Fe, Fe_3B, and Nd-oxides. This oxygen induced dissociation reaction is different from a common oxidation of metal where the oxygen atoms diffuse into the crystal lattice and form an oxide. This dissociation may occur by direct reaction with oxygen at the surface, thus the oxidation (or dissociation) rate of the $Nd_2Fe_{14}B$ compound crystal may be less likely to depend on the crystallographic orientation. The oxidized layer on surface of $Nd_2Fe_{14}B$ compound crystal has a unique morphology. Fig. 4 shows the morphology of oxidized layer formed on the surface of the $Nd_2Fe_{14}B$ crystal. The oxidized layer appears to consist of alternating needle-like bright and dark regions, which are more or less perpendicular to the interface between $Nd_2Fe_{14}B$ crystal matrix and oxidized layer (Fig. 4(B)). Composition of the bright and dark regions was analyzed by EDS in SEM, and the results were shown in Table 1. The contents in Table 1 were obtained by taking an average value from ten different spots. Together with XRD results, this compositional analysis indicates that both the bright and the dark regions are composed of multi-phase mixture of α-Fe, Fe_3B, and Nd oxides, and the bright region is

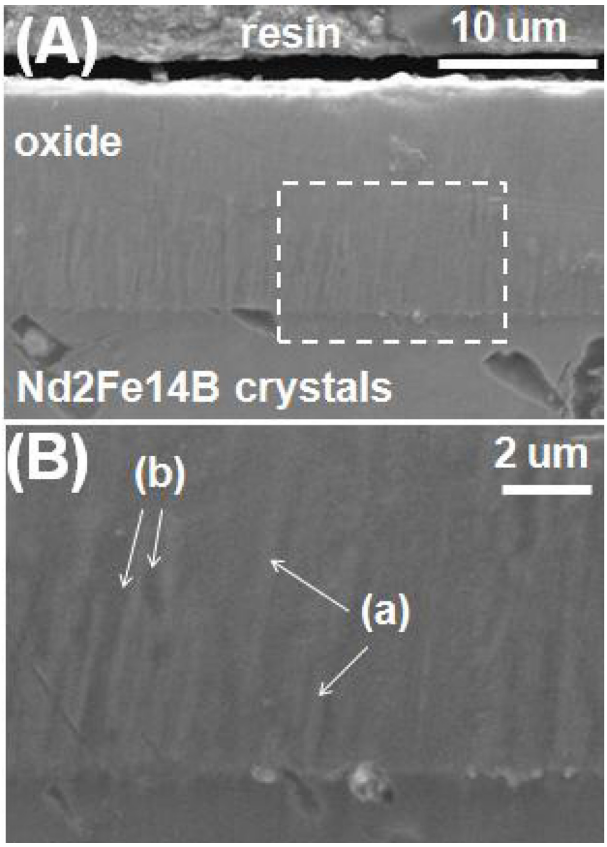

Fig. 4. SEM photos showing the morphology of the oxidized layer on the $Nd_2Fe_{14}B$ crystal grains in the $Nd_{15}Fe_{77}B_8$ alloy oxidized at 723 K for 3 hrs. (B) is zoom-in image of the area indicated by dash line square in (A).

Table I. Chemical composition of the regions (spot (a) and (b) in Fig. 4(B)) in the oxidized layer (wt%).

SPOT	Nd	Fe	O
a	25.45	64.73	9.82
b	24.73	67.21	8.06

enriched slightly with Nd oxides, while the dark region is enriched slightly with α-Fe.

Fig. 5 shows the variations of oxidized layer thickness as a function of exposing time to air for the $Nd_2Fe_{14}B$ crystal grains in the $Nd_{15}Fe_{77}B_8$ alloy oxidized at various temperatures. It appears that the oxidized layer thickness increases linearly with exposing time. Considering the continuous and dense-looking oxidized layer, the linear relationship of oxide layer thickness against exposing time would seem to be somewhat unexpected. It is common that the increase of oxide layer thickness follows the parabolic rate law rather than the linear relationship particularly when the formed oxide layer is dense and continuous. For the oxidation with dense and continuous layer, the oxidation rate is controlled predominantly by

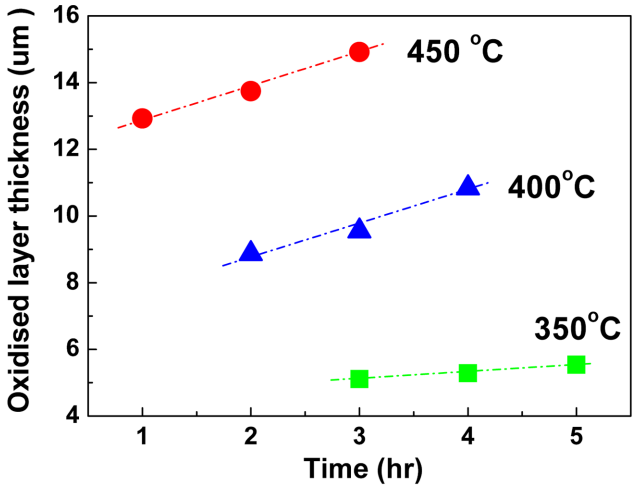

Fig. 5. (Color online) Variations of oxidized layer thickness as a function of exposing time to air for the $Nd_2Fe_{14}B$ crystal grains in the $Nd_{15}Fe_{77}B_8$ alloy oxidized at various temperatures.

the diffusion of oxygen through the oxide to the interface between oxide and crystal, and this type of reaction becomes non-steady-state diffusion-controlled reaction and shows typical parabolic rate law. In the present study, however, the increase of oxidized layer thickness with exposing time shows unexpectedly a linear relationship rather than a parabolic rate law. The linear relationship suggests that the oxidation rate is not controlled by the diffusion of oxygen through the oxidized layer to the interface of oxidized layer and crystal core but controlled predominantly by the direct reaction between the oxygen and crystal at the interface. This linear relationship implies that the reaction product (oxidized layer) does not act as a diffusion barrier for the oxygen. Oxygen may move easily to the interface between oxidized layer and crystal through a diffusion along the phase boundary between the different constituting phases in the oxidized layer. Thus, overall oxidation rate may be controlled predominantly by the direct reaction between the oxygen and crystal at the interface. The oxidation reaction can, therefore, be modeled according to simple linear relationship:

$$D = k_{ox}t + C \quad (1)$$

where D is the oxide layer thickness, k_{ox} is the linear oxidation rate constant, t is the time, and C is a constant. The dependence of k_{ox} on the temperature, T, is given by the Arrhenius equation:

$$k_{ox} = A\ exp - E/RT \quad (2)$$

where A is a constant of the frequency factor, E is the activation energy for the oxidation reaction, and R is the gas constant. Activation energy, E, for this oxidation

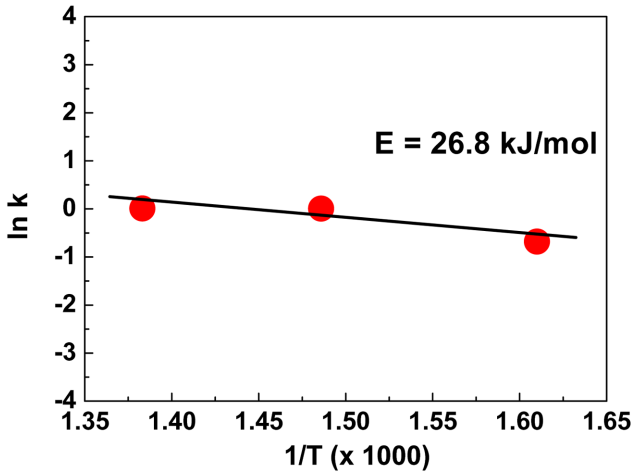

Fig. 6. (Color online) Plot of ln k_{ox} against $1/T$ for the oxidation of $Nd_2Fe_{14}B$ crystal.

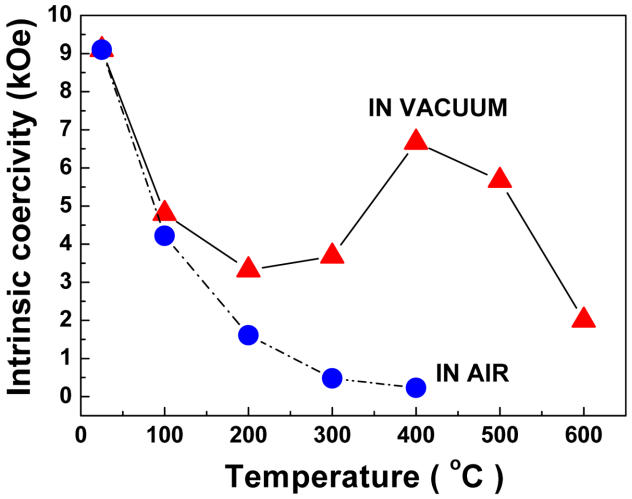

Fig. 7. (Color online) Coercivity variation as a function of heating temperature in air or vacuum for the fine $Nd_2Fe_{14}B$ crystal particles.

reaction can be determined by taking the logarithm of both sides of Eq. (2), and then plotting the ln k_{ox} against the reciprocal of the absolute temperature. Then a straight line having slope equal to [*E/RT*] will result (Fig. 6), and the activation energy can be calculated from the slope. The activation energy for the oxidation of $Nd_2Fe_{14}B$ compound crystal was estimated to be approximately 26.8 kJ/mol. This activation energy is much smaller compared to the previously reported values (around 100 kJ/mol) [4]. In this reference, the oxidation kinetics was studied by measuring the oxidized layer on the surface of bulk magnet rather than on the $Nd_2Fe_{14}B$ crystal grain. In the bulk magnet, the $Nd_2Fe_{14}B$ crystal grains are surrounded by a continuous Nd-rich grain boundary phase, and this may retard the oxidation of the $Nd_2Fe_{14}B$ crystal grain. While, in the present study, the $Nd_2Fe_{14}B$ crystal grain was exposed directly to oxygen, thus the oxidation occurred more rapidly, hence leading to a lower activation energy. Besides, in the reference the oxidation was undertaken at higher temperature for much longer period of time. The characteristics of the oxidized layer in that reference may be significantly different from that in the present work, and this may account for the significantly different activation energy.

The annealed $Nd_{15}Fe_{77}B_8$ alloy exhibits no coercivity because the $Nd_2Fe_{14}B$ crystal grains in the annealed ingot have grain size much larger than the critical single domain size (≒0.3 μm) of the $Nd_2Fe_{14}B$ crystal. In order to exploit high coercivity in the $Nd_2Fe_{14}B$ crystal particles, the particle size need to be reduced down to the size comparable with the critical single domain size. Fine $Nd_2Fe_{14}B$ crystal particles in near single domain size was prepared by ball milling of the HDDR-treated $Nd_{15}Fe_{77}B_8$ alloy, and these particles were used for investigating the effect of oxidation on the coercvity. The prepared near single domain size $Nd_2Fe_{14}B$ crystal particles (≒0.3 μm) had high coercivity over 9 kOe. However, the coercivity was radically reduced as the temperature increased in air (< 2 kOe at 200 °C) (Fig. 7). This radical coercivity reduction was attributed to the soft magnetic phases, α-Fe and Fe_3B, which were formed on the surface of the fine particles due to the oxidation. The magnetic soft phases (α-Fe, Fe_3B) at the surface of fine $Nd_2Fe_{14}B$ crystal particle may act as a nucleation site of reverse domain, hence facilitating demagnetisation and reducing coercivity radically. Meanwhile, when the prepared fine particles were heated in vacuum the coercivity increased significantly from 300 °C, peaking at 400 °C. This may be attributed to the removal of internal strain which was caused by mechanical damage during the ball milling.

IV. Conclusion

Oxidation of the $Nd_2Fe_{14}B$ compound crystal occurred by dissociation of the $Nd_2Fe_{14}B$ phase into multi-phase mixture of α-Fe, Fe_3B, and Nd oxides. Oxidation rate of the $Nd_2Fe_{14}B$ compound crystal showed no dependence on the crystallographic direction. The oxidation reaction was modeled according to simple linear relationship. Activation energy for the oxidation of $Nd_2Fe_{14}B$ compound crystal was calculated to be approximately 26.8 kJ/mol. The near single domain size $Nd_2Fe_{14}B$ crystal particles (≒0.3 μm) had high coercivity over 9 kOe. However, the coercivity was radically reduced as the temperature increased in air (< 2 kOe at 200 °C). This radical coercivity reduction was

attributed to the soft magnetic phases, α-Fe and Fe_3B, which were formed on the surface of the fine particles due to the oxidation.

Acknowledgement

The author H.W. Kwon would like to acknowledge that the present work was supported by Pukyong National University Research Promotion Program (2011).

References

[1] J. J. Croat, J. F. Herbst, R. W. Lee, and F. E. Pinkerton, J. Appl. Phys. **55**, 2078 (1984).
[2] M. Sagawa, S. Fujimura, N. Togawa, H. Yamamoto, and Y. Matsuura, J. Appl. Phys. **55**, 2083 (1984).
[3] Y. Li, H. E. Evans, I. R. Harris, and I. P. Jones, Oxidation of Metals **59**, 167 (2003).
[4] I. Skulj, H. E. Evans, and I. R. Harris, J. Mater. Sci. **43**, 1324 (2008).
[5] W. Q. Liu, M. Yue, G. P. Wang, D. T. Zhang, and J. X. Zhang, Corrosion **66**, 0550041 (2010).
[6] J. I. Lee, H. W. Kwon, and Y. S. Kang, J. Magnetics **13**, 102 (2008).